PHYSICAL REVIEW B VOLUME 59, NUMBER 16 15 APRIL 1999-II

Resonant charge transfer in ion–metal surface collisions: Effect of a projected band gap in the H^--Cu(111) system

A. G. Borisov
Laboratoire des Collisions Atomiques et Moléculaires (Unité de Recherches Associée au CNRS 281), Université Paris-Sud, Bâtiment 351, 91405 Orsay Cedex, France

A. K. Kazansky
Institute of Physics, Saint Petersburg University, St. Petersburg 198904, Russia

J. P. Gauyacq*
Laboratoire des Collisions Atomiques et Moléculaires (Unité de Recherches Associée au CNRS 281), Université Paris-Sud, Bâtiment 351, 91405 Orsay Cedex, France

(Received 27 July 1998; revised manuscript received 12 October 1998)

A wave-packet propagation method is applied to the treatment of the resonant charge transfer (RCT) process in the interaction between an H^- ion and a Cu(111) surface. Using a model description of the Cu(111) electronic structure, it is shown that the RCT efficiency is deeply influenced by the presence of the Cu(111) projected band gap, that partially blocks the electron transfer in the direction normal to the surface. The differences between the RCT process on a free electron metal surface and on a Cu(111) surface are discussed. The two cases are associated with very different pictures of the electron transfer. In particular, the importance of the Cu(111) surface state for the decay of the H^- ion is demonstrated. The effect of the band gap is also shown to strongly depend on the interaction time. For short interaction times (large collision velocities), the electron wave packet does not have enough time to probe the metal band structure and the RCT on a Cu(111) surface is very similar to that on a free electron surface. For long interaction times (low collision velocities), the RCT efficiency is drastically reduced by the presence of the band gap. The wave-packet propagation method is also used to discuss the validity of the rate equation approach in the case of a free electron metal target. [S0163-1829(99)04415-X]

I. INTRODUCTION

During an atom (molecule)-metal surface collision, the interaction between the atomic and metallic electronic clouds can lead to a variety of phenomena, among which the atom (molecule)-surface charge transfer process has a special importance. It determines the charge state of atomic (molecular) particles reflected or sputtered from the surface, and it is also very often invoked as an important step in reaction mechanisms. When the charge transfer involves a one-electron transition between a projectile level and metallic levels of the same energy, it is called resonant charge transfer (RCT). When it is energetically possible, it is usually assumed to dominate over the other charge transfer processes, because of its one-electron-transition character.[1–6] This is, in particular, the case for the neutralization of alkali positive ions[7–10] or negative ion formation.[11–15] Owing to its importance, the RCT process has received a lot of interest both experimentally and theoretically.[1–6]

On the theoretical side, the interaction between the projectile discrete state and the continuum of metal states is usually described using an Anderson-Newns Hamiltonian.[1–6] Within several approximations for the treatment of the system dynamics (broad continuum band, high temperature, high parallel collision velocity, semiclassical conditions), one can show that the RCT process dynamics is governed by a rate equation where the electron transfer rates are given by the widths of the projectile states coupled with the continuum of metallic states.[16–20] A very significant progress in the quantitative treatment of the RCT followed the development of a few nonperturbative methods to determine the energies and widths of the projectile states in front of metal surfaces.[21–27] All these methods use a free electron (jellium) description of the metal target. The electrons are assumed to be free and independent inside the metal with which they interact via a local potential. Within this approximation, the charge transfer corresponds to the tunnelling of the active electron through the potential barrier separating the atomic potential well and the metal. Because of this tunnelling, the atomic states become quasistationary and acquire a finite lifetime τ, the inverse of their width Γ. In the case of free electron metals, these nonperturbative methods have been proved to be very efficient, they can quantitatively account for the experimental observations. As examples, one can mention the negative ion formation or the alkali ion neutralization processes.[10,13–15]

However, the situation could be rather different for non-free-electron metals. Indeed, one can expect the resonant charge transfer process to be affected by the three-dimensional (3D) electronic band structure of the metal target. For example, the case of a narrow band or of the band edge effect have been discussed within model studies.[28–30] Similarly, the properties of negative ion resonances in the case of molecules physisorbed on metals have been found to depend on the description (free electron or more realistic) of the metal surface.[31] The presence of a projected band gap in the direction normal to the surface similar to the *L* gap in the case of the Cu(111) surface should also have dramatic effects. Indeed, the electronic transitions between the metal surface and the atomic projectile are favored along the surface normal going through the projectile centre, where the potential barrier that the electron has to tunnel through is more transparent. Then, in the free electron case, the atomic level is preferentially coupled with the metallic states associated to a **k** momentum along the surface normal. This is directly observed in the distribution of the electrons emitted by the decay of an atomic level among the possible **k** states.[32] If the projectile level energy is above the Fermi energy and inside the *L* gap of Cu(111), an electron leaving the projectile along the surface normal will be reflected back from the potential inside the bulk Cu. In other words, the conduction band states which are *a priori* the most coupled with the projectile levels are absent in the case of a Cu(111) surface. This should be expected to lead to a drastic decrease of the charge transfer couplings.

We present a theoretical study of the resonant charge transfer between an H^- ion and a model Cu(111) surface. The main goal of this work is to analyze the peculiarities of the RCT dynamics induced by the presence of the projected band gap. In this purpose, the results obtained with the model Cu(111) surface are compared with those obtained with a free electron (jellium) metal of similar characteristics. The H^- ion has been chosen as a test projectile, since its unique level is located inside the Cu L-band gap. We analyze both the case of an H^- ion at a fixed distance from the surface and that of an H^- ion moving in front of the surface. Although not directly corresponding to an experimental situation, these two studies allow a discussion of the RCT process dynamics. Below, we demonstrate that the RCT is deeply affected by the presence of the projected band gap. Not only is the strength of the charge transfer coupling reduced, but also, the qualitative picture of the electron transfer is modified as well as the dynamics of the process.

The charge transfer dynamics is studied with the wave-packet propagation (WPP) method, developed for surface problems by Ermoshin and Kazansky.[25] It consists in following the time evolution of the wave function of the active electron induced by the charge transfer interaction. It is a very powerful method which can be used in two different contexts. In the static situation (fixed projectile-surface distance) one can obtain the atomic levels characteristics (energy and width). One can also directly study the dynamics of the RCT by following the wave-packet evolution during the projectile motion in front of the surface. The WPP method provides the exact solution of the dynamical problem and is free of the approximations one usually has to resort to, in order to be able to treat the collision dynamics. In particular, it naturally includes the nonadiabatic effects. This feature is used below to test the validity of the rate equation approach for the resonant charge transfer process. One of the further advantages of this method is illustrative: one can directly look at the electronic wave packet at different times during the evolution and so get a picture of the evolution. For all these advantages, the WPP method has been used in a variety of different processes and physical situations.[24,33–38] A short account of this work has already been presented in Ref. 39.

Below, Sec. II presents the models used to describe the charge transfer system and Sec. III is devoted to the wave-packet propagation technique. In Sec. IV, the results for static studies (fixed atom-surface distance) are discussed in detail, while Sec. V presents the study of the collision dynamics. Finally Sec. VI presents a few concluding remarks.

II. PRESENTATION OF THE MODELS

The basis of our approach is to look at the time evolution of the wave function of the electron active in the resonant charge transfer process. It is evolving in a compound potential that we take as the superposition of the electron-hydrogen core and electron-surface interaction potentials. Since the projectile core is neutral, we neglect the modification of the electron-surface interaction potential due to the presence of the projectile core. The assumption that the electron-projectile core and electron-surface potentials are additive forbids the application of this approach to the small ion-surface distance region, where the projectile core (hydrogen atom) and the surface strongly overlap.

For the description of the H^- ion, we use an open shell description with a loosely bound electron outside of a more compact neutral core. The outer electron is the active one in the RCT process and it interacts with the neutral core via a model potential we took from Ref. 40:

$$\mathcal{U}(r) = -(1+1/r)\exp(-2r) - (\alpha/2r^4)\exp(-\beta/r^2), \quad (1)$$

where r is the electron-hydrogen distance and the potential is given in atomic units. α, the hydrogen atom polarizability, is equal to $4.5a_0^3$ and β is equal to $2.547a_0^2$. The accuracy of the wave-packet propagation method that we use quickly decreases when the potential becomes very large. Therefore, the potential has been regularized in order to avoid the singularity of the potential when r goes to zero.[25]

For the surface, we studied two different models: one model in which there exists a projected band gap and a free electron model. This allows a direct analysis of the band gap effect.

The free electron model is identical to the one used in our previous studies.[10,13–15] The electron interacts with the surface via a potential of the form given by Jennings *et al.*[41] It is only a function of z, the electron-surface distance, measured from the surface image reference plane ($z>0$ is the vacuum side):

$$\begin{aligned} V_{e\text{-surf}}(z) &= -[1-\exp(-\lambda z)]/4z, \quad z>0, \\ V_{e\text{-surf}}(z) &= -V_0/[1+A\exp(Bz)], \quad z<0. \end{aligned} \quad (2)$$

Here, λ is equal to $1.5a_0^{-1}$ and V_0 is equal to 11.61 eV (the potential is referred to the vacuum level). The other parameters are such that the potential (2) and its derivative are continuous on the surface. The above definition puts the origin for the z coordinate on the image reference plane. This is the origin for all the distances from the surface in this work. Below, this first model is called the jellium Cu model.

The second model, which is referred to as model Cu(111), has been constructed along the lines of earlier works.[42,43] It has been designed to reproduce the gross features of the Cu(111) surface. It consists of a local potential that is periodic along the z axis inside the metal (the $\langle 111\rangle$ direction)

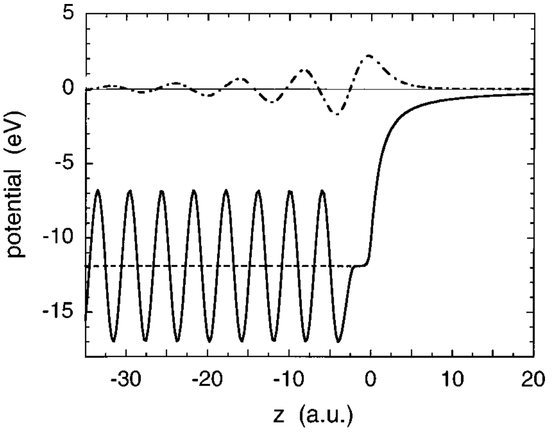

FIG. 1. Model potentials used to represent the electron-model Cu(111) interaction (solid line) and the electron Cu jellium interaction (dashed line), as a function of z, the electron coordinate normal to the surface. $z=0$ corresponds to the position of the image plane. The dashed dotted line represents the wave-function for the surface state.

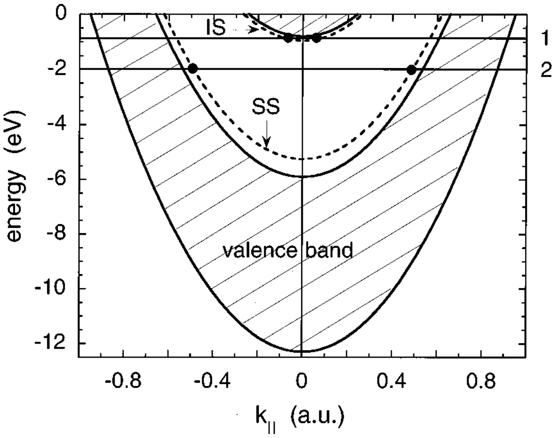

FIG. 2. Schematic picture of the Cu(111) electronic structure as a function of the electron momentum parallel to the surface. The shaded area represents the 3D valence band continuum. The dashed lines labeled SS and IS represent the surface state and the first image state, respectively.

and joins a potential of the form (2) outside the metal. The potential is taken independent of the two coordinates parallel to the surface. It has the following form:

(a) $Z<Z_0-\pi/G$,

$$V_{e\text{-surf}}(z)=-V_0+V_G\cos[G(Z-Z_0)], \tag{3a}$$

(b) $Z_0-\pi/G<Z<Z_0$,

$$V_{e\text{-surf}}(z)=-V_0-0.5V_G\{1-\cos[G(Z-Z_0)]\}, \tag{3b}$$

(c) $Z>Z_0$,

$V_{e\text{-surf}}(z)$ is given by Eq. (2), where $G=1.596a_0^{-1}$. This potential only contains the first harmonic of the 3D potential corresponding to G, the reciprocal lattice vector in the (111) direction. It opens an L band gap located between -5.9 and -0.8 eV, for $V_G=2.55\,\text{eV}$.[42] The matching distance $Z_0=-2.0106a_0$ and the λ parameter in Eq. (2) have been adjusted so that the surface state and the first image state energies in the model (-5.25 and -0.96 eV, respectively) reproduce the characteristics of the Cu(111) surface.[42] Our potential (3) is very close to the one reported for Cu(111) in Ref. 44. However, the two models slightly differ in the way the matching between Eqs. (2) and (3) is performed. The full potential as a function of z is presented in Fig. 1, together with the surface state wave function. The surface state wave function peaks in the surface region and quickly decreases inside the vacuum. In the bulk metal, it decays exponentially while oscillating with the reciprocal lattice vector period.

The electronic structure of the model Cu(111) surface is schematically displayed in Fig. 2. It shows the energy of the electronic levels as a function of k_{par}, the electron momentum parallel to the surface. Within the present model, the electron movement is free in the direction parallel to the surface, leading to free electron dispersion curves in Fig. 2. In the real Cu(111) surface, the dispersion curves of the band gap boundaries and of the surface state are associated with an effective mass of $0.42m_e$, whereas the image state dispersion curve corresponds to an effective mass of $1m_e$.[42] We do not think that this simplification in our model affects the qualitative features of the H$^-$-Cu(111) charge transfer process. The H$^-$ outer electron energy is equal to -0.75 eV in the free ion and it decreases when the ion approaches the metal surface due to the image charge attraction. The H$^-$ ion level is then located inside the L band gap of the surface. It is degenerated and coupled with a few metallic states: (i) the first image state continuum for large ion-surface distances (situation 1 in Fig. 2); the ion state is degenerated with the image state with a well defined k_{par}, (ii) the surface state continuum for not too small ion-surface distances (situations 1 and 2); the ion state is degenerated with the surface state with a well defined k_{par}, (iii) the valence band continuum: the H$^-$ level is degenerated with the valence band states with k_{par} above a certain threshold value. The dimensions of these continua are different: 2D for the surface state and the image state and 3D for the valence band. However, the invariance of the problem by rotation around the atomic axis normal to the surface decreases by one the dimension of the continua effectively coupled with the H$^-$ ion level.

The degeneracy with the image state continuum only occurs at large ion-surface distances where the RCT coupling is weak and so this situation is not much discussed below. For an intermediate Z range, the H$^-$ level is degenerated with states in both the valence band and the surface state continuum associated with a finite k_{par}. In the case of a free electron metal, the H$^-$ ion level is degenerated with continuum states having all kinds of k_{par} momenta and is mainly coupled with those around $k_{\text{par}}=0$. In the case of the Cu(111) model, the absence of continuum states degenerated with the ion level and associated with a vanishing k_{par} should lead to a drastic change in the RCT efficiency.

III. WAVE-PACKET PROPAGATION METHOD

Before describing the WPP procedure, we will make some further remarks on the RCT in the H$^-$-Cu(111) system. The surface work function of the Cu(111) surface is rather high (4.94 eV) compared to the H$^-$ binding energy. For the hydrogen-surface distances considered here, the H$^-$ level is degenerated with unoccupied metal states and the RCT can be expected to only result in electron loss by the negative ion (the situation would be different in the case of fast grazing collisions where the so-called parallel velocity effect[45] can bridge the gap between the Fermi level and the H^- level). The purpose of the present work is mainly to analyze the characteristics of the RCT process induced by the presence of the band gap. We only consider the hydrogen motion normal to the surface, thus reducing the problem to electron loss by the ion and we only treat the evolution of a unique electron in the compound potential formed by the atom and the surface. Indeed in a real H^--Cu(111) collision, both electron capture and loss would exist and the final ion fraction would reflect the balance between the two processes.

The wave-packet propagation method consists in studying the time evolution of an electron wave packet in the compound potential defined in the previous section. The time-dependent electron wave function $\psi(\mathbf{r},t)$ is a solution of the time-dependent Schrödinger equation with the Hamiltonian *H*. The initial electron wave function $\psi(\mathbf{r},0)$ is taken equal to $\psi_a(\mathbf{r})$, the eigenfunction of the potential (1), i.e., the free H^- ion wave function. Within the chosen model, the system is invariant by rotation around *Oz*, the axis normal to the surface and going through the hydrogen center. We therefore use cylindrical coordinates (z is the coordinate along the symmetry axis, ρ is the distance to this axis, and ϕ the azimuth angle). Since the free H^- ion level is spherical, we only have to study the $m=0$ case (m is the projection of the electron angular momentum on the symmetry axis).

We have found that the convergence of the time propagation scheme is improved by the following change of function:

$$f(\mathbf{r},t)=\sqrt{\rho}\,\psi(\mathbf{r},t). \tag{4}$$

Substitution of Eq. (4) into the time-dependent Schrödinger equation yields

$$i\,\frac{df(\mathbf{r},t)}{dt}=\tilde{H}f(\mathbf{r},t) \tag{5}$$

with

$$\tilde{H}=T_Z+T_\rho+V_{e\text{-}H}(\mathbf{r})+V_{e\text{-surf}}(z), \tag{6}$$

where

$$T_Z=-\frac{1}{2}\,\frac{d^2}{dz^2} \tag{7a}$$

and

$$T_\rho=-\frac{1}{2\sqrt{\rho}}\,\frac{d}{d\rho}\left(\rho\,\frac{d}{d\rho}\right)\frac{1}{\sqrt{\rho}}. \tag{7b}$$

The time propagation of the electron wave function is obtained via the evolution operator $U(\Delta t)$:

$$f(\mathbf{r},t+\Delta t)=U(\Delta t)f(\mathbf{r},t), \tag{8a}$$

where

$$U(\Delta t)=\exp(-i\tilde{H}\Delta t). \tag{8b}$$

The Hamiltonian $\tilde{H}$ is independent of time in the static case (fixed ion-surface distance). In the dynamic case, it becomes time dependent through the time dependence of the potentials (the ion is supposed to follow a classical trajectory in front of the surface). In that case, the Hamiltonian in Eq. (8) is evaluated at the time $(t+0.5\Delta t)$. For the evolution operator, we use the split operator approximation[46–48]

$$U(\Delta t)=\exp\left(-i\tilde{H}_1\frac{\Delta t}{2}\right)\exp(-i\tilde{H}_2\Delta t)\times\exp\left(-i\tilde{H}_1\frac{\Delta t}{2}\right)+0(\Delta t^3), \tag{9}$$

where

$$\tilde{H}_1=T_Z+V_{e\text{-}H}(\mathbf{r})+V_{e\text{-surf}}(z)$$

and

$$\tilde{H}_2=T_\rho. \tag{10}$$

The exponential operators in Eq. (9) are calculated using the unitary and unconditionally stable Cayley scheme[49,50]

$$\exp(-i\tilde{H}\Delta t)=\frac{1-i(\Delta t/2)\tilde{H}}{1+i(\Delta t/2)\tilde{H}}+0(\Delta t^3). \tag{11}$$

The electron wave function is discretized on a grid of points in cylindrical coordinates

$$z\in[-z_{\min},z_{\max}]\equiv[-140.5,99.5]$$

and

$$\rho\in[0,100]\ \ \text{(in atomic units)}. \tag{12}$$

The origin of the coordinates is placed at the H^- ion center. The z_j mesh points are equally spaced with a step Δz equal to $0.2a_0$. For the ρ coordinate, we first perform the change of variable $\rho=x^2$ and use equally spaced points x_i with a step Δx equal to $0.02a_0^{1/2}$.

The operators are discretised using a three-point differentiation scheme

$$(\tilde{H}_1 f)_{i,j}=\frac{-1}{2(\Delta z)^2}[f_{i,j+1}+f_{i,j-1}-2\,f_{i,j}]+V_{e\text{-}H}(r_{i,j})+V_{e\text{-surf}}(z_j), \tag{13a}$$

$$(\tilde{H}_2 f)_{i,j}=\frac{-1}{8x_i^2(\Delta x)^2}\times\left[\frac{x_i+\Delta x/2}{x_i+\Delta x}f_{i+1,j}+\frac{x_i-\Delta x/2}{x_i-\Delta x}f_{i-1,j}-2\,f_{i,j}\right], \tag{13b}$$

where the $f_{i,j}$ and $r_{i,j}$ quantities are evaluated at the (x_i,z_j) mesh point. Given the above discretisation, the inverse operator in Eq. (11) is obtained by the Cranck-Nicholson algorithm[50] via the solution of a tridiagonal set of equations, with the boundary condition of a vanishing function on the grid boundary: $f_{i,j}=0$ (for *i,j* belonging to the grid boundaries).

During the propagation, part of the electron wave packet goes into the metal and spreads over the entire grid. The presence of grid boundaries *a priori* results in artifact reflections of the wave packet: the electron that has escaped from the H^- ion and gone into the bulk metal is reflected on the grid boundary and goes back to the hydrogen. To cancel these spurious reflections and keep a pure outgoing wave behavior for the electron wave packet, we have introduced an absorbing potential[51–54] near the grid edges. Consistently with the presence of the absorbing potential, the electron wave function is set equal to zero on the grid boundary. It has been checked that large variations in the absorbing potential characteristics do not induce in general any variation of the physical quantities, thus confirming its role as only imposing a pure outgoing wave boundary condition.

In the static problem, one studies the electron dynamics for a fixed ion-surface distance, with the initial electron wave function equal to $\psi_a(\mathbf{r})$. The wave-packet propagation scheme then provides $\psi(\mathbf{r},t)$, from which we define the survival amplitude in the free ion bound state or equivalently, the electronic wave-packet autocorrelation function

$$A(t)=\langle\psi_a(\mathbf{r})|\psi(\mathbf{r},t)\rangle \tag{14}$$

and its Laplace transform

$$g(\omega)=\frac{1}{\pi}\int_0^\infty dt e^{i\omega t}A(t)=\frac{1}{\pi}\int_0^\infty dt e^{i\omega t}\langle\psi_a(\mathbf{r})|\psi(\mathbf{r},t)\rangle. \tag{15}$$

The real part of $g(\omega)$ gives $n(\omega)$, the projected density of states (DOS). $n(\omega)$ presents a Lorentzian peak at the resonance position, i.e., at the energy of the quasibound state of H^-. It can be used to extract the resonance characteristics, i.e., the level energy (E) and width (Γ). However, this procedure is accurate only if the propagation is performed over a rather long time interval, until the wave packet has entirely left the atom in order to reach the convergence of the Laplace transform (15). This imposes extremely long propagation times in the case of very narrow resonances. In order to avoid long propagation times, we directly analyze the autocorrelation function as a superposition of a few exponential terms, the parameters of which are determined by a least square fit procedure:

$$A(t)=\sum_{j=1}^{L} a_j \exp\left\{-i\left(E_j-i\frac{\Gamma_j}{2}\right)t\right\}. \tag{16}$$

In the present case, the number of structures in the projected density of states is rather limited, so that an excellent convergence of the fit can be reached with $L=3$. With this procedure, we can determine resonance widths in the 10^{-3} eV range with a time propagation over only 1500–2000 a.u., i.e., with a decay of the initial wave packet smaller than 10%. An alternative method for accurately determining the resonance characteristics while avoiding long time propagation is the filter diagonalization method.[55–57] It has been proven to be extremely efficient in the case of a large number of quasistationary states.

In the dynamical calculations, we consider an hydrogen atom moving with respect to the surface at a constant velocity v, according to the trajectory

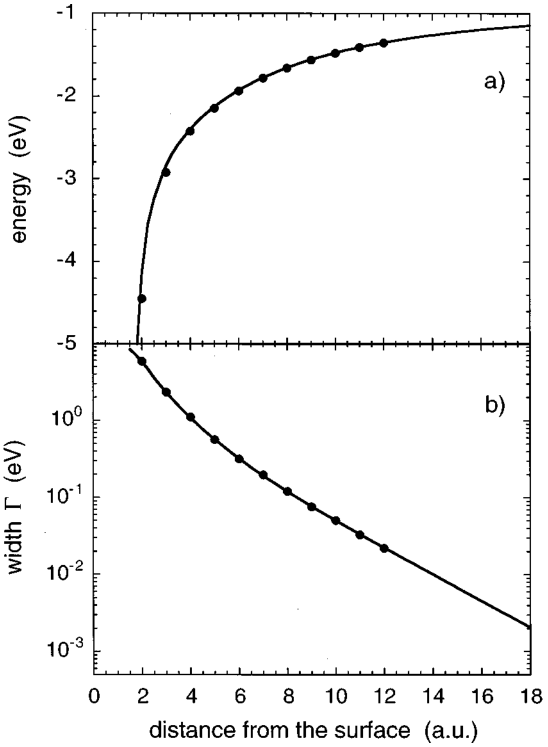

FIG. 3. Energy position (a) and width (b) of the H^- level in front of a Cu jellium surface, as a function of the ion-surface distance, measured from the image plane. The full line represents the results obtained with the CAM method and the black dots those obtained with the wave-packet propagation method.

$$Z(t)=Z_{\min}+|Z_{\max}-Z_{\min}-\nu t|, \quad 0<t<T, \tag{17}$$

where

$$T=2(Z_{\max}-Z_{\min})/\nu.$$

Z is the hydrogen-surface distance. The electron wave packet $\psi(\mathbf{r},t)$ is initially equal to $\psi_a(\mathbf{r})$. $Z_{\max}$ is taken large enough so that the H^- ion can be considered as free. Then, after propagation over the $[0,T]$ interval, we get the survival probability of the ion in the course of the collision or at the end of the collision $P(t)=|A(t)|^2$. In the propagation, we neglect the effect on the electronic wave packet of the sudden change of direction in the trajectory at $T/2$. First, in a real trajectory, the change in the trajectory would not be so abrupt. Second, this approximation makes easier the comparison between the wave packet propagation predictions and the rate equation predictions.

IV. RESULTS FOR THE STATIC PROBLEM

A. Energy and width of the ion level

Figures 3(a) and 3(b) present the energy position and width of the H^- ion level interacting with the surface in the jellium Cu case. The results are very similar to those obtained for the H^- ion level (or other negative ion levels) interacting with a jellium metal surface.[13,58] For such a loosely bound system such as H^-, the ion level characteristics in front of a jellium only very slightly depend on the jellium characteristics.[58] The electron binding energy is found to increase when the ion approaches the surface,

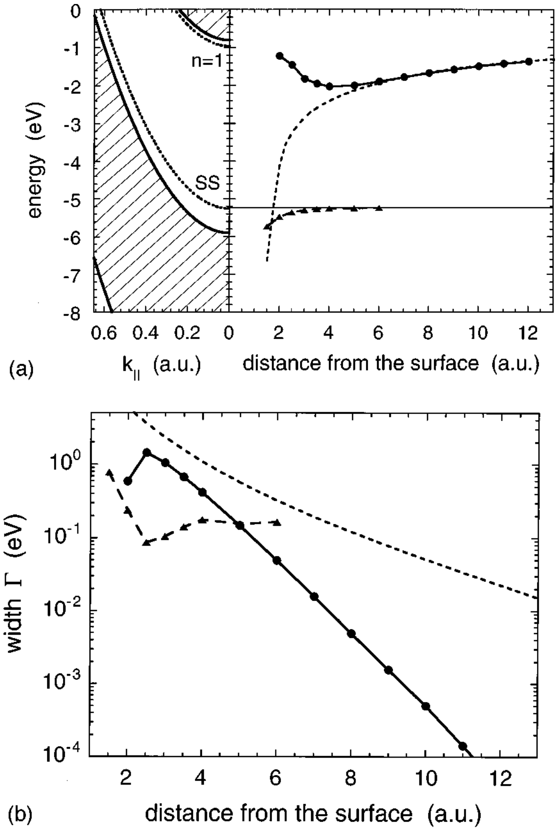

FIG. 4. (a) Energy position of the H^- ion level in front of the model Cu(111) surface as a function of the ion-surface distance. Dashed line: jellium Cu results. Lines with symbols: results for the model Cu(111) surface. The horizontal thin line is located at the energy position of the bottom of the surface state continuum. The left part of the figure presents the electronic structure of Cu(111) as a function of the electron momentum parallel to the surface. (b) Width of the H^- ion level in front of a model Cu(111) surface as a function of the ion-surface distance. Short dashed line: jellium Cu results. Lines with symbols: results for the model Cu(111) surface. Solid line with black dots: width of the highest lying resonance. Long dashed line with black triangles: width of the lowest lying resonance.

roughly following the image potential variation. The level width displays an exponential behavior with the ion-surface distance Z, reaching very large values, in the eV range, at small distances. Figure 3 presents the results obtained with the wave-packet propagation technique compared with those obtained with the coupled angular mode (CAM) method.[22] The two sets of results are almost identical, even at small Z, where the magnitude of the width makes the definition of the quasistationary state rather difficult. This confirms the validity of the two approaches to determine the level energy and width. It must be stressed that the two methods are very different, although they address the same basic problem: the determination of the characteristics of resonant scattering by a potential. In the CAM method, one studies the stationary scattering problem, whereas, the wave-packet propagation method studies the nonstationary problem of the time evolution of the electron wave function under the action of the potential.

Figures 4(a) and 4(b) present the energy position and width of the H^- ion level interacting with the surface in the model Cu(111) case. The situation appears rather different from that of the jellium Cu case. The level width [Fig. 4(b)] exhibits an exponential behavior with Z for large distances, however, it is much smaller than in front of the jellium surface. This is the direct consequence of the existence of the band gap: the metal levels which contribute most to the level width in the jellium case (those with k_{par} around zero) are absent in the model Cu(111) case. The slope of the $\Gamma(Z)$ function is different in the two calculations. The Z behavior of the width is linked with the exponential decrease into the vacuum of the metal states involved in the RCT, i.e., the states degenerated with the H^- state. The exponential tails of the metal states are given by their energy component normal to the surface: $E_z = E_a - (1/2)k_{\mathrm{par}}^2$, where E_a is the energy of the H^- ion level. In the jellium case, the ion state interacts mainly with the metal states corresponding to $k_{\mathrm{par}} = 0$, so that E_z is practically equal to the ion energy and varies with the ion surface distance (typically in the range -1, -2 eV). In contrast, in the model Cu(111) case, we have found that the ion state mainly interacts with the surface state which corresponds to a fixed E_z equal to -5.25 eV. This difference in E_z accounts for the difference in the $\Gamma(Z)$ slope.

In the large Z region, the level energy [Fig. 4(a)] is found to roughly follow the image charge variation, very close to the behavior of the jellium Cu case. This is not surprising either, the level energy shift can be estimated from the value of the potential at the centre of the ion and in both models, the potential in this region is equal to the image charge interaction. The two models strongly differ in the small Z region. In the model Cu(111) case, a second resonance is present at low energy and a transfer of amplitude in the projected density of states occurs from high-energy to low-energy resonance as the distance Z decreases (see the discussion of Fig. 6 below). It appears that the ionic level, the energy of which is decreasing when Z decreases, cannot cross the threshold of the surface state. An avoided crossing appears and a new state moves away from below the surface state threshold. The importance of the surface state threshold results from the dominant role played by the surface state continuum in the H^- ion decay. These aspects can be further stressed by looking at the projected density of states.

B. Projected density of states

Figure 5 presents the projected density of states $n(\omega)$ in the jellium Cu case for an ion-surface distance Z equal to $6a_0$. On the logarithmic scale, the ion level appears as a sharp quasi-Lorentzian peak sitting on top of a flat background. The position and width of the peak yield the energy and width of the quasistationary state. The background covers the jellium continuum: it drops sharply at the bottom of the continuum, below V_0 [Eq. (2)] and more slowly above the vacuum level. Note that the shape and importance of the background depends on the initial wave function used in the calculations.

Figure 6 presents the projected density of states in the model Cu(111) case for various ion-surface distances. At large distances, the ionic level corresponds to the highest peak in the spectrum. It must be noticed that these large Z calculations were performed with a limited propagation time T. The use of a Laplace transform over a too small time

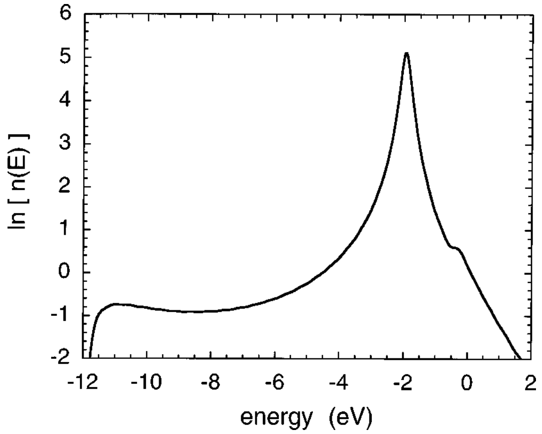

FIG. 5. Logarithm of the projected density of states for the case of an H^- ion interacting with a jellium Cu surface. The ion surface distance is 6 a.u.

interval generates oscillations in the projected density of states. To smoothen out these oscillations, we used a Gaussian filtering of the autocorrelation $A(t)$ with a half width equal to $T/2$. This artificially broadens the $n(\omega)$ structures, so that small level widths are not properly described and the ion level peaks are not as sharp as they should. Moreover, the optical potential used at the grid boundaries can also increase the level width in the case of long lived states associated with wave functions much spread in space. The large Z spectra also show a few structures in the background, which stress the Cu(111) band structure. At low energy, the background drops sharply at the bottom of the valence band with a structure associated with the threshold. Similar threshold structures are visible around -5.2 and -1 eV and are attributed to the surface state and first image state thresholds. The existence and importance of these background structures are directly linked with the wave-packet propagation procedure. Indeed, for a fixed Z distance, the initial wave packet is chosen as $\psi_a(\mathbf{r})$. For a finite Z, the wave function corresponding to the quasistationary state is not exactly equal to the free ion wave-function, so that the initial wave packet also contains contributions from all the continuum states leading to the background visible in Figs. 5 and 6. Changing the initial wave-packet results in variations of the relative importance of the various structures, although without altering the ionic level characteristics (energy and width).

The evolution of the ionic resonance is quite visible at small Z. The high-energy resonance correlated at infinity with the free ion level roughly stays at the same place, it has a decreasing importance in the projected DOS when Z decreases. The peak spreads and becomes difficult to be separated from the image state threshold. At the same time, a new resonance appears below the surface state threshold and gains amplitude as Z decreases. The ionic character is then found to transfer from high-energy resonance to the low-energy one. As a direct consequence of the choice of the initial wave packet, we can mainly obtain the characteristics of the resonances with a large ionic character and this explains why the characteristics of the two resonances are determined in limited Z domains.

The behavior of the atomic resonance obtained in our model Cu(111) study can be understood by analysing the threshold law of the interaction between the ionic and the

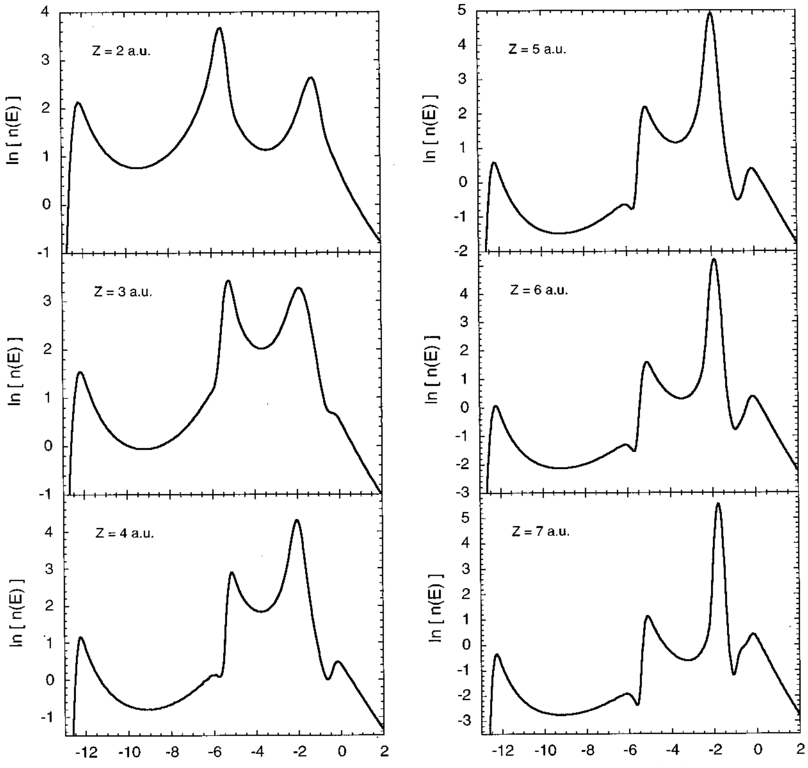

FIG. 6. Logarithm of the projected density of states for the case of an H^- ion interacting with a model Cu(111) surface. The various pictures correspond to different ion-surface distances Z.

surface states. Let us first consider the case of the interaction between a discrete state of energy E_0 and a continuum of states parametrised with the energy ε. Following Fano's interaction configuration view of this problem,[59–61] the energy of the quasistationary state is given by the solution E of the equation

$$E = E_0 + P\int_0^{\infty} d\varepsilon \frac{|V_{0\varepsilon}|^2}{E-\varepsilon}, \tag{18}$$

where P stands for the Cauchy principal part of the integral and $V_{0\varepsilon}$ is the interaction between the discrete and continuum states. In the case of a degenerate continuum, one has to sum the squared modulus of the interactions over the degeneracies. The surface state is a two-dimension continuum and so, the threshold law for the interaction is such that the sum of $|V_{0\varepsilon}|^2$ over the degeneracies goes to a constant when ε goes to 0^+. As a consequence, the shift function $\Delta(E)$,

$$\Delta(E) = P\int_0^{\infty} d\varepsilon \frac{|V_{0\varepsilon}|^2}{E-\varepsilon}, \tag{19}$$

has a logarithmic divergence for E going to zero. For negative energies, the shift function $\Delta(E)$ is negative and monotonous, it behaves as A/E for large negative E. Thus, Eq. (18) always has a solution for negative energies, i.e., there always exists a bound state for such a problem, even if E_0 is positive. For small discrete state-continuum interactions, the binding energy becomes exponentially small.[6]

The behavior at positive energies depends on the behavior of the interaction $V_{0\varepsilon}$ as a function of ε. That can lead to the existence of zero, one or more resonances. This situation is a direct consequence of the interaction threshold law at the continuum boundary (band edge effect). The appearance of a bound state below the continuum threshold in the case of strong discrete state-continuum interactions has also been found in the context of chemisorption studies.[42,62] In addition, it has also been discussed in model studies of the charge transfer process in atom-surface collisions in the case of narrow bands,[28,29] as well as in the case of electron scattering by polar molecules (see, e.g., Ref. 63).

To describe the behavior of the atomic resonance in the model Cu(111) case, we first neglect the valence band continuum and only discuss the interaction between the surface state and the ionic state, which exactly corresponds to the situation analyzed above. For large Z, the coupling with the surface state continuum is small and the atomic resonance is at the expected energy, imbedded in the surface state continuum. At the same time, as soon as the ion level–surface state continuum coupling is nonzero, there exists a bound state just below the surface state continuum. It is difficult to see in the projected DOS (Fig. 6) since it is very close to threshold and has only a very small component on the free ionic state. As Z decreases, the ionic level approaches the threshold and the charge transfer coupling increases, leading to an increase of the binding energy of the state below the surface state threshold as well as to an increase of the ionic component in its wave function. For very small Z, where one expects from the image charge attraction that the ionic state is below the surface state threshold, most of the ionic amplitude appears to be transferred to the lowest lying state and the upper resonance is more difficult to see. Indeed, in Fig. 4(a) the energy of the lowest resonance is seen to decrease at very small Z where it has gained most of the ionic character. At the same time, the energy of the highest resonance is slightly increasing, confirming the avoided crossing character of the interaction between the two resonances. The above interpretation concerns a discrete state crossing a continuum boundary. It appears that the resonant state located inside the continuum cannot cross the continuum threshold to transform into a bound state. Although the atomic character is transferred from the upper resonance to the lower one, they do not correlate to each other.

In the above discussion, we only considered the coupling between the H^- ion level and the surface state continuum. In fact, the situation is more complex since the discrete state is also coupled and imbedded in the valence band continuum. As a result, the low lying state that appears below the surface state continuum is not a real bound state but a resonance with a finite width since it can decay into the valence band continuum. At large Z, its width, as given in Fig. 4(b), is in the 0.1 eV range. However, this width is not the actual level width, which is much smaller. At large Z, the lowest resonance corresponds to a bound movement along the ρ coordinate with a very small binding energy with respect to the bottom of the surface state continuum. Its wave function is extremely spread along ρ and overlaps the absorbing potential in the outer part of the grid. This brings a spurious absorption which dominates at large Z and is responsible for the constant value of the width computed in this region. At very small Z, the lowest resonance is very low in the projected band gap so that the blocking effect of the gap is weak and decreases as Z decreases, leading to the observed increase of the level width.

C. Wave packets as functions of time

Figures 7(a)–7(c) present the electronic wave packet at three different times, 0, 50, and 600 a.u. for the jellium Cu case (the atomic unit of time is equal to $2.42\ 10^{-17}\,\mathrm{s}$). The ion is at a fixed distance $(7a_0)$ from the surface. The origin of the coordinates is located at the ion centre. The logarithm of the modulus of the electron wave packet is plotted as a function of the z and ρ coordinates. In Fig. 7(a), one sees $\psi_a(\mathbf{r})$, the bound state of the free H^- ion. After a short time [Fig. 7(b)] the wave packet has slightly changed, it has expanded in the direction of the metal, corresponding to the decay of the H^- ion by emitting an electron into the metal. It is noticeable that the outgoing flux of the electron is mainly concentrated along the surface normal where the tunnelling between the ion and the metal is easier, i.e., metal states with k_{par} around zero are populated. One can also notice that for such a short time, the electron did not have time to go far into the metal and the bump around $z=-30a_0$ corresponds to the wave front of the electron wave packet going into the metal. Later in the evolution [Fig. 7(c)], an important part of the wave packet has already gone into the metal and one has reached a steady state equilibrium inside the metal with an electron flux from the ion to the metal in the direction perpendicular to the surface. One still notices that the decay of the wave packet is mainly concentrated in the small ρ region around the surface normal. The oscillations with a large pe-

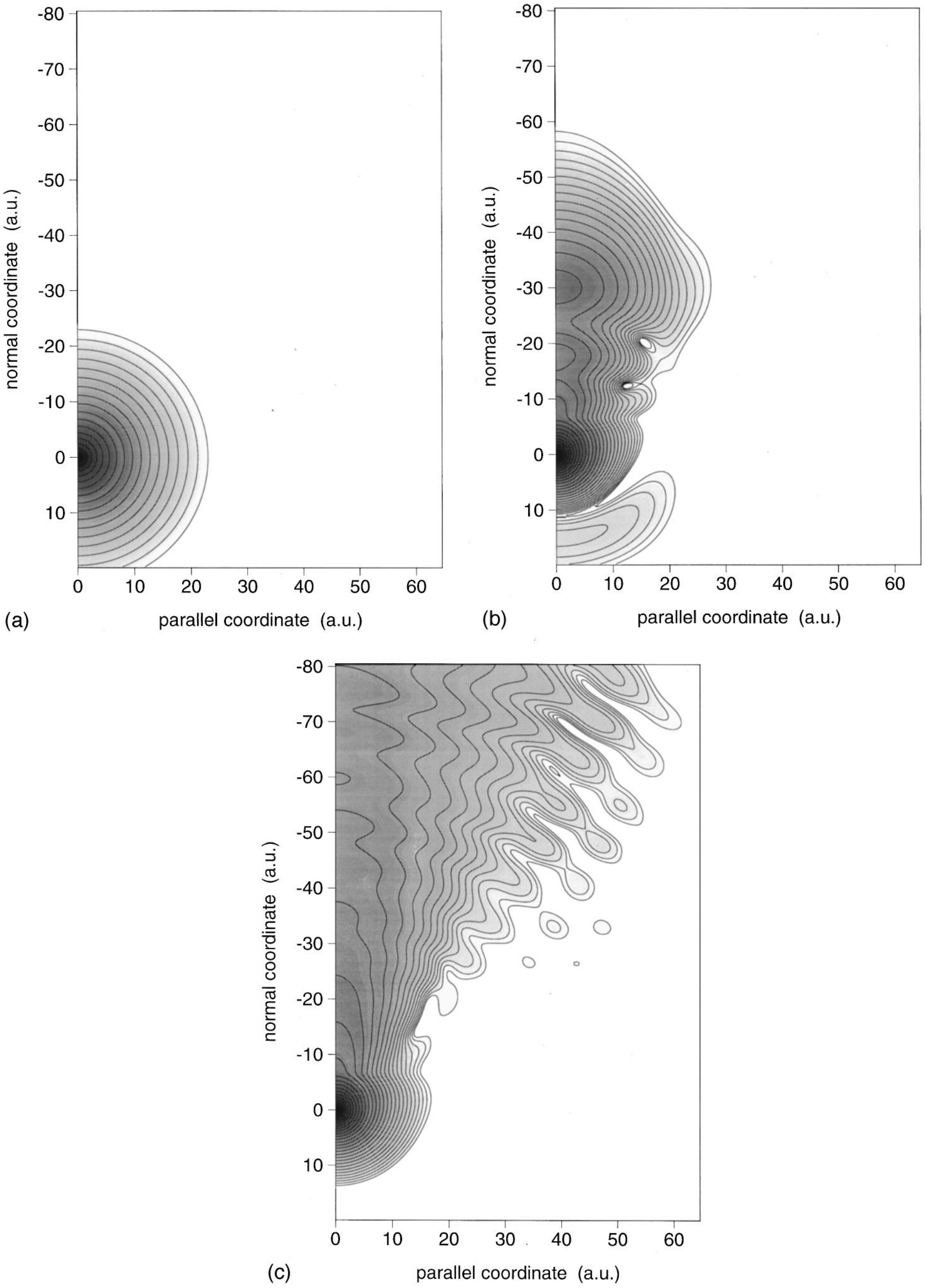

FIG. 7. (a) Logarithm of the modulus of the initial electron wave packet in the static WPP calculation as a function of the z and ρ electron coordinates, respectively, normal and parallel to the Cu surface. The ion-surface distance Z is fixed and equal to 7 a.u. and the origin of coordinates is at the ion center. The grey scale is used to represent the variation of the wave-packet modulus (the dark region corresponds to the maximum of the wave packet). The black rings join points with equal values of the wave-packet modulus; their spacing corresponds to a variation of one of the logarithm of the wave-packet modulus. (b) Logarithm of the modulus of the electron wave packet after a propagation time of 50 a.u. in the case of a jellium Cu surface (static WPP calculation at $Z=7$ a.u.). See caption of Fig. 8(a). (c) Logarithm of the modulus of the electron wave packet after a propagation time of 600 a.u. in the case of a jellium Cu surface (static WPP calculation at $Z=7$ a.u.). See caption of Fig. 8(a).

riod around $10a_0$ seen on the figure are attributed to the interference between the outgoing wave leaving the quasistationary state and a background contribution. This background is related to the initial projection of the wave packet on the eigenfunctions of the entire Hamiltonian, generating components on the quasistationary state (the Lorentzian peak in the DOS) and on all the continuum states (the background in the DOS).

The case of the WP evolution for the model Cu(111) surface presented in Figs. 8(a) and 8(b) is quite different. For a short time ($t=50$ a.u.), one can see that the electron wave packet has gone from the ion into the metal, mainly along the surface normal. However, the wave packet now exhibits a series of oscillations in the z direction. These are a direct consequence of the band gap existence. The decay of the H^- ion mainly populates the surface state continuum and the

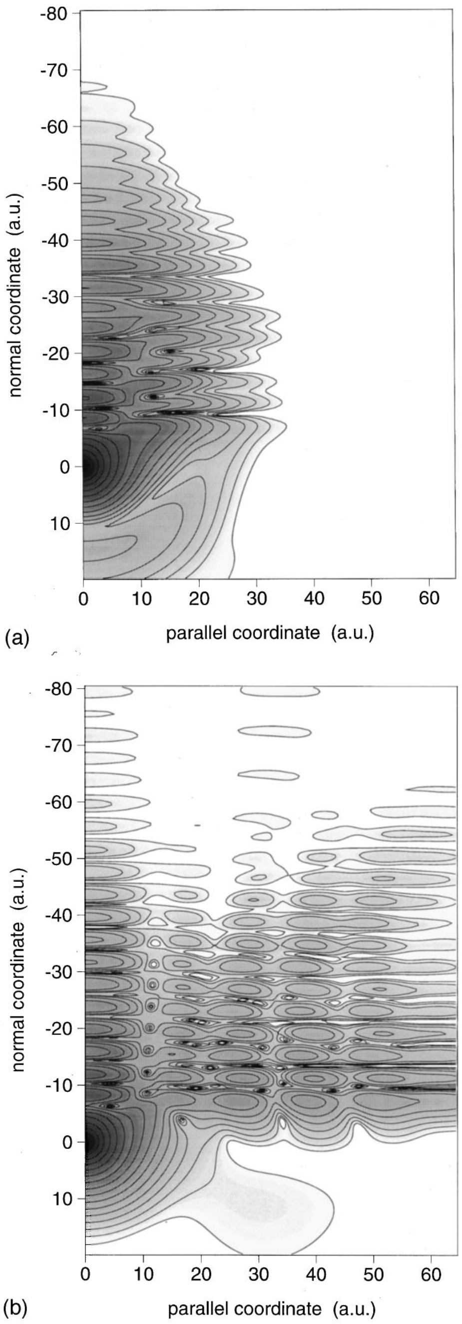

FIG. 8. (a) Logarithm of the modulus of the electron wave packet after a propagation time of 50 a.u. in the case of a model Cu(111) surface (static WPP calculation at $Z=7$ a.u.). (b) Logarithm of the modulus of the electron wave packet after a propagation time of 1000 a.u. in the case of a model Cu(111) surface (static WPP calculation at $Z=7$ a.u.). See (a).

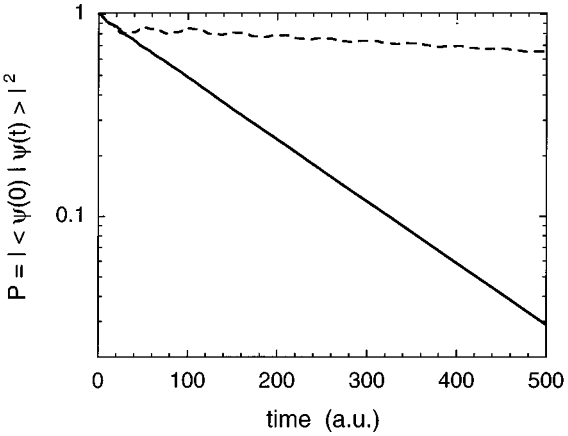

FIG. 9. Survival probability (squared modulus of the autocorrelation function) as a function of time for an H^- ion placed at a distance of 7 a.u. from the surface. Full line: jellium Cu case. Dashed line: model Cu(111) case.

wave-packet shape inside the metal reflects the wave function of the surface state (see Fig. 1) and corresponds to free motion along the ρ coordinate. The electron has tunneled from the ion to the metal along the surface normal. Owing to the reflectivity of the potential inside the bulk, the electron cannot go deep into the metal and builds the surface state wave function which then spreads along the ρ coordinate. This spreading parallel to the surface can be seen on Fig. 8(b) which corresponds to a late time where a steady state flux out of the ion has been reached ($t=1000$ a.u.). One can recognize the surface state wave function along the z direction and the flux of electrons moving away in the ρ direction. The electron density deep into the metal is very weak, corresponding to the penetration of the surface state (see Fig. 1).

The above description of the dynamics only refers to the ion decay to the surface state continuum. In fact, there is also a small probability of decay of the ion into the valence band. In that case, metal states with a minimum k_{par} are populated, i.e., the electrons are emitted beyond a certain angle from the surface normal. This threshold angle is slightly visible in the upper right corner of Fig. 8(b); in fact, the structure along an oblique line corresponds to the interference between the two decays into the surface state and into the valence band continua. The oscillations appearing along the ρ direction are attributed to interferences with the wave-packet background as well as to interferences between the two quasistationary states appearing in this case (see above discussion of Fig. 6). From Figs. 7(b), 7(c), 8(a), and 8(b), one can see that the decay of the H^- ion is quite different in the two cases: in the jellium case, the emitted electron is moving mainly along the surface normal, whereas, in the model Cu(111) case, it does not penetrate deep into the metal and moves away parallel to the surface.

D. Short time behavior

From the above analysis of the width of the level, one can expect the time behavior of the H^- ion survival probability to be quite different in the two cases [jellium and model Cu(111)], the decay being much faster in the jellium case. The situation is not exactly like that, in particular for the short time behavior. The survival probability $P(t)$ for the H^- ion as a function of time is presented in Fig. 9 for the two models and for an ion-surface distance Z of $7a_0$. In the long time region, one recognizes the two exponential decays corresponding to the two very different widths for the ion level in the two models. The situation at short time is, however, different. Below 15–20 a.u. (around 0.4 fs), the ion decays in the same way in the two models, the decay rate corresponding to the width in the jellium case. Then, the decay curve

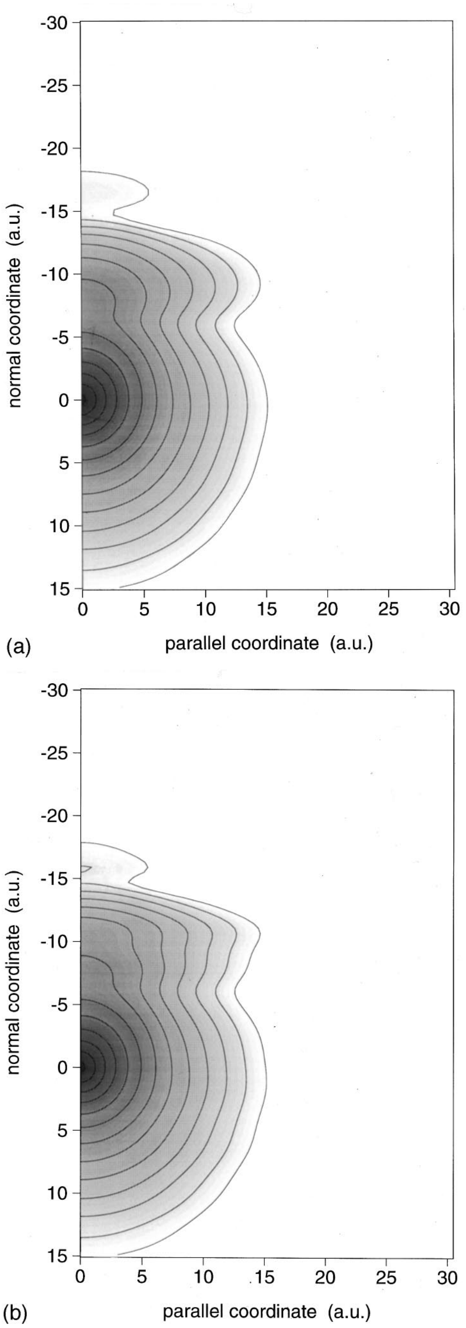

FIG. 10. Logarithm of the modulus of the electron wave packet after a propagation time of 10 a.u. (static WPP calculation at $Z=7$ a.u.). (a) presents the case of a jellium Cu surface and (b), that of the model Cu(111) surface. See caption of Fig. 8(a).

for the model Cu(111) case splits from that of the jellium case while presenting a few oscillations and switches to the exponential decay associated with the width of the model Cu(111) case. This feature can be further outlined by looking at the electron wave packet in this short time domain. Figure 10 presents the two wave packets for the jellium and model Cu(111) cases at $t=10$ a.u.: they are practically identical, confirming that the beginning of the ion decay is the same in the two cases.

This short time behavior can be interpreted in the following way. In the model Cu(111) case, at the beginning of the decay, the electron leaves the ion and tunnels through the barrier where the transparency is the highest, i.e., along the surface normal. At that time, the electron wave packet has not yet probed the periodic variation of the potential inside the metal and then it behaves as in the jellium case. The complete reflectivity of the surface in the band gap is due to the interference between all the waves reflected by the various atomic planes. Therefore, it takes some time before the electron wave packet penetrates inside the metal and experiences the oscillations in the potential, so that the destructive interference can lead to the reflection of the electron wave packet. Then the wave packet comes back toward the ion and after a few of these movements, the surface state wave function appears and it is only then that the ion level decays according to its static width. The oscillations in the survival probability on Fig. 9 are attributed to these electronic movements that build the surface state wave function.

The time required by the system to switch from one behavior to the other can be interpreted in two ways. First, it can be linked to the travel time of the electron between the surface plane and the atomic planes. Indeed, the time needed by an electron with an energy around 10 eV to go back and forth between the surface and the first maximum in the potential in Fig. 1 is around 15 a.u. So, the building time for the surface state wave function is of the order of a few of these back and forth movements. The duration of the short time behaviour can also be linked to the band gap width through the uncertainty relation. If one looks at the system on a short time scale, an energy uncertainty appears that can cancel the gap effect. In Fig. 9, the ionic level is located around -1.8 eV, i.e., around 1 eV from the upper gap edge. This energy difference corresponds to a time around 30 a.u. These two views of the short time period should indeed be equivalent through a time-energy uncertainty relation. The above two time estimates, which are of the same order of magnitude as the time limit observed on Fig. 9, should not be considered as accurate, they are just a way of illustrating the existence of a short time limit.

From this, one can conclude that the effect of the band gap on the charge transfer needs time to become operative. It must be stressed that the static width corresponds to an infinite time study of the level dynamics. On a short time scale, when the electron emitted by the ion has not yet ''explored'' the bulk band structure, the ion decay is the same as in the jellium case. The system evolves with the width determined in the static calculations only after a finite time. As shown below, this affects the dynamics of the charge transfer in a collision problem if the collision time is of the order of magnitude of the duration of the short time region.

V. RESULTS OF THE DYNAMICAL STUDY

In our dynamical study, an incident H^- ion approaches the surface from infinity down to a minimum distance $Z_{\min}$ and then goes back to infinity. We vary independently the collision velocity v and the distance of closest approach $Z_{\min}$ to elucidate the dynamics of the RCT process on Cu(111). Therefore, $Z_{\min}$ does not correspond to the actual turning point of the trajectory for an H^- ion of velocity v colliding on a Cu(111) surface. It must be considered as a ''theoretical experiment'' designed to stress the peculiarities of the RCT process on a Cu(111) surface. Within the wave-packet propa-

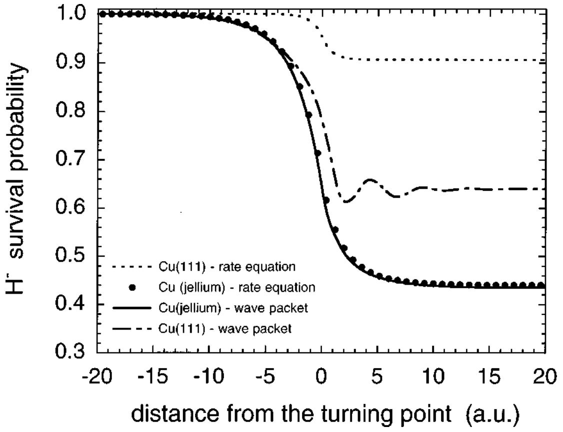

FIG. 11. Survival probability along the trajectory for an H$^-$ ion colliding with a Cu surface at a normal velocity of 0.1 a.u. The turning point of the trajectory is located at 5 a.u. from the surface. The horizontal distance scale corresponds to distance to (from) the turning point of the trajectory. The negative (positive) distances correspond to the incoming (outgoing) part of the trajectory. Full line: dynamical WPP calculation in the jellium Cu case. Black dots: rate equation prediction in the jellium Cu case. Dashed dotted line: dynamical WPP calculation in the model Cu(111) case. Dotted line: rate equation prediction using the static rates for the model Cu(111) case.

gation approach, we directly follow the time evolution of the electronic wave function during this collision. Below, we use the wave-packet propagation results as a reference against which we test the predictions of the rate equation approach. In the latter approach, the time evolution of the ion level population is governed by the width $\Gamma(Z)$ of the level

$$\frac{dP}{dt} = -\Gamma[Z(t)]P(t). \tag{20}$$

Equation (20) leads to the following solution for the negative ion survival probability at the end of a complete collision with a turning point at $Z_{\min}$ (trajectory followed with a constant velocity ν):

$$P(\infty) = \exp\left(-\frac{2}{\nu} \int_{Z_{\min}}^{\infty} \Gamma(Z')dZ' \right). \tag{21}$$

Figure 11 presents the results obtained for the ion population $P(t)$ along the trajectory for a collision velocity of 0.1 a.u. and a turning point of the trajectory located at $Z_{\min} = 5a_0$. Two sets of results are shown for the jellium Cu case: the wave-packet propagation and the rate equation results. The two curves are almost identical, confirming the validity of the rate equation approach for a jellium surface. The ion population steadily decreases along the trajectory with a symmetric behavior around the turning point since the ion decay is purely local. The relevance of the level width for the description of the RCT process for a one-electron problem has already been proved using a wave-packet propagation method within a simple 1D model of the system.[64]

The result for the model Cu(111) surface is quite different. At the beginning of the collision, the ion decay is almost identical to that found in the Cu jellium case. However, after some time, the survival probability departs from the jellium result and presents some oscillations as a function of time. These oscillations are attributed to electron reflections by the atomic planes in the Cu bulk which build up the surface state wave function. Roughly speaking, at the beginning of the collision, the ion decay is fast and governed by the jellium rate, whereas, after the surface state wave function has built up, the decay is much slower, breaking the symmetry between the two parts of the collision. As a result, the survival probability at the end of the collision is significantly larger in the model Cu(111) case than in the jellium case. For comparison, we have also evaluated the prediction of the rate equation using the H$^-$ static width obtained in the Cu(111) model [adiabatic state given by the full line with black dots in Fig. 4(b)]. It is found to be quite different from the wave-packet propagation results, in particular in the first half of the collision. So, for this velocity regime, we find that the charge transfer dynamics in the model Cu(111) case is not governed by the static width of the ion level, the H$^-$ survival probability at the end of the collision is much smaller than predicted by the rate equation approach using this static width.

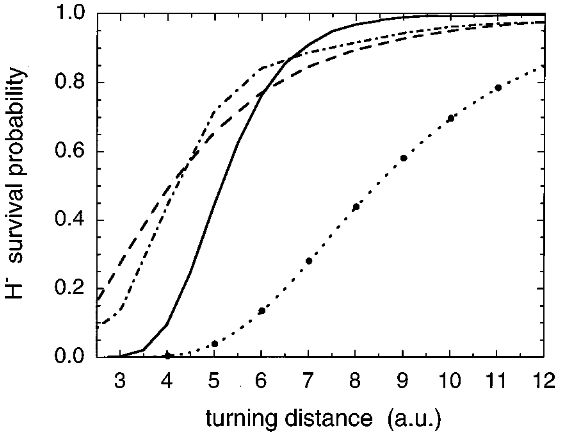

FIG. 12. Final survival probability at the end of the collision for an H$^-$ ion colliding with a model Cu(111) and jellium Cu surfaces. It is presented as a function of the distance between the trajectory turning point and the surface. The various lines corresponds to different collision velocities v. Results for the model Cu(111) surface: $v = 0.2$ a.u. (dashed line); $v = 0.05$ a.u. (dashed dotted line); $v = 0.0125$ a.u. (full line). Results for the jellium Cu surface with a collision velocity of 0.025 a.u.: results of the dynamical WPP calculation (black dots); results of a rate equation approach (dotted line).

Further illustration can be found by looking at the final survival probability at the end of the collision, as a function of the turning point of the trajectory. This does not correspond to a quantity that can be experimentally observed, since in a real system, for a given collision energy, there is a well defined turning point. Looking at the survival probability as a function of the turning point is only for analysis purpose. It allows us to analyze the dynamics of the RCT as a function of the strength of the charge transfer coupling: the closer from the surface is the turning point, the larger the charge transfer coupling is. Figure 12 presents the results for the survival probability as a function of the turning point for a few situations. For the jellium case (collision velocity 0.025 a.u., i.e., collision energy around 16 eV), as expected, the survival probability decreases when the turning point comes closer to the surface, i.e., when the charge transfer

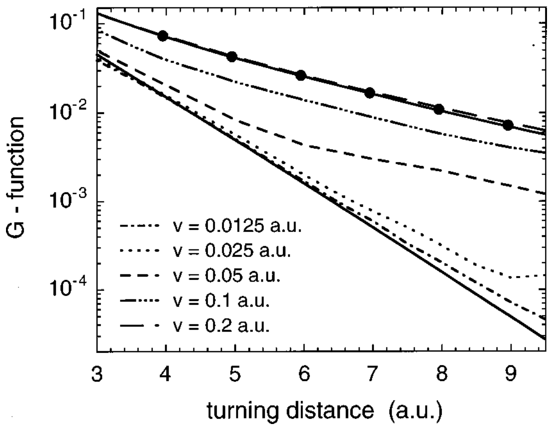

FIG. 13. G quantity as a function of the turning point of the trajectory. Upper and lower full lines: predictions of a rate equation approach using the jellium Cu and model Cu(111) level widths, respectively. Black dots: WPP results for the jellium Cu case ($v=0.1$ a.u.). Broken lines: WPP results for the model Cu(111) case and various collision velocities (see inset).

coupling increases. Figure 12 compares the results obtained within the wave-packet propagation technique and obtained within the rate equation approach for the Cu jellium case. The two results are found to be almost identical, once again confirming the validity of the rate equation approach in the jellium case.

Figure 12 also presents the survival probability as a function of the turning point for various collision velocities, obtained in the model Cu(111) case. The variation of this quantity with the turning point is qualitatively the same as for the jellium surface, the electron loss increases when the ion approaches the surface. However, the velocity dependence is nonmonotonous. On the contrary, in the rate equation approach, with a constant velocity, Eq. (21) predicts a monotonous behavior of the survival probability with the collision velocity: it decreases when the collision velocity decreases. This corresponds to the fact that the charge transfer process can be described as the exponential decay of the ionic state into the continuum: within this picture, the longer is the interaction time, the larger is the decay. This behavior is qualitatively seen in Fig. 12 for the smallest Z_{min}, however, it is almost inverted in the large Z_{min} region. There the electron loss seems to rather have a dynamical behavior: it is increased by the collision velocity. To further stress this point we have defined the following effective quantity G:

$$G=(-\nu/2)\ln[P(\infty)]. \tag{22}$$

In the wave-packet propagation approach, G *a priori* depends on the turning point of the trajectory Z_{min} and on the collision velocity. However, in the rate equation approach, from Eqs. (21) and (22), the quantity G is independent of the collision velocity and reduces to the integral of the level width over the ion-surface distance from Z_{min} to infinity. It is not an experimentally observable quantity, but is very useful in the model Cu(111) case to analyze the departure of the RCT dynamics from that of the rate equation approach. The G quantity obtained from the wave-packet propagation is shown on Fig. 13 as a function of the turning point Z_{min} for various collision velocities. Figure 13 also shows the integral of the level width over the distance in the jellium and model Cu(111) cases. It is found that G is much dependent on the collision velocity, confirming that the dynamics of the electron transfer in the H-Cu(111) system cannot be described by a simple rate equation. At the smallest collision velocity ($v=0.0125$ a.u. corresponding to a collision energy around 3.9 eV), the G quantity almost coincides with the integral of the level width in the model Cu(111) case. Then, the electron wave packet has enough time to probe the entire electron-metal surface interaction potential and thus it evolves with the level width obtained in infinite time static calculations. In contrast, for the largest velocity ($v=0.2$ a.u., i.e., a collision energy of 1 keV), the G quantity is very close to the integral of the width of the H^- level in front of a Cu jellium surface. For such a fast collision, the electron does not have enough time to probe the surface potential deep in the metal and its evolution is simply governed by the outer part of the electron-metal surface potential which is identical in the model Cu(111) and Cu jellium cases. Figure 13 also shows the results obtained from the wave-packet propagation in the jellium Cu case for a collision velocity of 0.1 a.u., they are almost identical to the integral of the level width. This is quite consistent with the results in Fig. 12.

VI. CONCLUDING SUMMARY

We presented the results of a study of the H^--Cu(111) surface resonant charge transfer process using the wave-packet propagation technique for both a jellium and a model description of the surface. It has revealed a very strong effect of the Cu(111) projected band gap. The H^- ion level lies inside the band gap and this results in an important decrease of the level width, i.e., of the strength of the charge transfer coupling. However, it also appears that this level width is not the only relevant quantity governing the RCT dynamics. In certain cases the charge transfer on the Cu(111) target can be as efficient as in the case of a jellium metal target. This confirms that the dynamical evolution of a system cannot always be deduced from the knowledge of its static description.

The behavior of the H^--Cu(111) system is very original, due to the interplay of the electron tunnelling through the potential barrier and the reflectivity of the surface in the band gap. The H^- level mainly decays into the surface state continuum rather than into the valence band continuum. This leads to a picture of the RCT which is quite different from that in the case of a jellium target. With a jellium surface, the transferred electron penetrates into the metal bulk along the normal to the surface, whereas for the Cu(111) case, the electron flux is first directed from the ion to the metal along the normal to the surface and then it turns away parallel to the surface, without penetrating deep into the Cu bulk.

The dynamical behavior of the system depends on the collision velocity. At small velocity, the system behaves according to its static width whereas at high velocity, the efficiency of the charge transfer is much increased and the Cu(111) surface becomes similar to a jellium surface. The electron needs a finite time to move into the metal and explore the bulk band structure, i.e., to ‘‘know’’ about the existence of the projected band gap. Before this, it behaves as in the jellium case. If the collision is fast enough, it is over before the electron had time to probe the surface properties and the RCT has the jellium characteristics.

The wave-packet propagation technique has been used as a reference to test the predictions of the rate equation approach in the case of a jellium metal target. Indeed, the wave-packet method provides an exact solution for the time evolution of the wave function of the active electron. The rate equation has been found to be extremely accurate for the jellium target. It should, however, be stressed that this test only concerns a one electron problem. The existence of a few active electrons can bring in many-body effects (see discussion in Ref. 6).

At small ion-surface distances, the interaction of the H$^-$ ion level with the model Cu(111) surface state leads to the existence of two resonances which share the ionic character. This aspect should bring nonadiabatic effects in the charge transfer process, i.e., direct transitions between the two resonances induced by the ion movement. Such nonadiabatic transitions are taken into account in an exact way within the wave-packet propagation approach. They would be rather similar to nonadiabatic effects which have been found in the case of charge transfer on adsorbate covered surfaces.[65–67] It can be stressed that the existence of important nonadiabatic effects should result in the loss of the resonant character of the one-electron charge transfer process: the atomic level decay cannot be described by a width and can populate continuum levels far away in energy from the atomic resonance.

A few aspects of the RCT problem in an H$^-$-Cu(111) collision have not been considered here: angular and energy distributions of the electrons ejected during the collision and appropriate treatment of the ion trajectory, in particular in the turning point region. These should be handled, possibly together with an improvement of the model description of the Cu, to allow a detailed comparison with experimental results. Nevertheless, from the above analysis, we can expect that a projected band gap does influence experimental results on electron capture (loss) in atom-surface collisions. Both the decrease of the charge transfer coupling for slow normal collision velocities and the change of behavior when the collision energy increases should have important consequences. It concerns the charge state of atomic (molecular) particles reflected (sputtered) from a metal surface as well as the many reactions at surfaces which imply a charge transfer step. In addition, as we have seen, the surface state continuum plays a dominating role in the charge transfer process. It is a 2D continuum in contrast with the 3D valence band continuum involved in the case of a free electron metal. It has been shown[68–69] that this change of dimension of the continuum strongly modifies the parallel velocity assisted charge transfer process[45] and can be observed in grazing angle atom scattering from surfaces.

---

*Author to whom correspondence should be addressed. FAX: 33-(0)1 69 15 76 71. Electronic address: gauyacq@lcam.u-psud.fr

[1] A. Yoshimori and K. Makoshi, Prog. Surf. Sci. **21**, 251 (1986).

[2] R. Brako and D. M. Newns, Rep. Prog. Phys. **52**, 655 (1989).

[3] A. Nourtier, J. Phys. (France) **50**, 311 (1989).

[4] J. J. C. Geerlings and J. Los, Phys. Rep. **190**, 133 (1990).

[5] J. Burgdörfer, in *Review of Fundamental Processes and Applications of Atoms and Ions*, edited by C. D. Lin (World Scientific, Singapore, 1993), p. 517.

[6] H. Shao, D. C. Langreth, and P. Nordlander, in *Low Energy Ion-Surface Interactions*, edited by J. W. Rabalais (Wiley, New York, 1994), p. 118.

[7] E. G. Overbosch, B. Rasser, A. D. Tanner, and J. Los, Surf. Sci. **93**, 310 (1980).

[8] G. A. Kimmel and B. H. Cooper, Phys. Rev. B **48**, 12 164 (1993).

[9] E. R. Behringer, D. R. Andersson, B. H. Cooper, and J. B. Marston, Phys. Rev. B **54**, 14 765 (1996).

[10] A. G. Borisov, D. Teillet-Billy, J. P. Gauyacq, H. Winter, and G. Dierkes, Phys. Rev. B **54**, 17 166 (1996).

[11] J. N. M. Van Wunnick, J. J. C. Geerlings, and J. Los, Surf. Sci. **131**, 1 (1983).

[12] F. Wyputta, R. Zimny, and H. Winter, Nucl. Instrum. Methods Phys. Res. B **58**, 379 (1991).

[13] A. G. Borisov, D. Teillet-Billy, and J. P. Gauyacq, Phys. Rev. Lett. **68**, 2842 (1992).

[14] M. Maazouz, A. G. Borisov, V. A. Esaulov, J. P. Gauyacq, L. Guillemot, S. Lacombe, and D. Teillet-Billy, Phys. Rev. B **55**, 13 869 (1997).

[15] C. Auth, H. Winter, A. G. Borisov, B. Bahrim, D. Teillet-Billy, and J. P. Gauyacq, Phys. Rev. B **57**, 12 579 (1998).

[16] A. Blandin, A. Nourtier, and D. Hone, J. Phys. (France) **37**, 369 (1976).

[17] W. Bloss and D. Hone, Surf. Sci. **72**, 277 (1978).

[18] R. Brako and D. M. Newns, Surf. Sci. **108**, 253 (1981).

[19] J. J. C. Geerlings, J. Los, J. P. Gauyacq, and N. M. Temme, Surf. Sci. **172**, 257 (1986).

[20] P. Nordlander and D. C. Langreth, Phys. Rev. B **43**, 2541 (1991).

[21] P. Nordlander and J. C. Tully, Phys. Rev. Lett. **61**, 990 (1988).

[22] D. Teillet-Billy and J. P. Gauyacq, Surf. Sci. **239**, 343 (1990).

[23] F. Martin and M. F. Politis, Surf. Sci. **356**, 247 (1996).

[24] J. Merino, N. Lorente, P. Pou, and F. Flores, Phys. Rev. B **54**, 10 959 (1996).

[25] V. A. Ermoshin and A. K. Kazansky, Phys. Lett. A **218**, 99 (1996).

[26] S. A. Deutscher, X. Yang, and J. Burgdörfer, Phys. Rev. A **55**, 466 (1997).

[27] P. Kürpick, U. Thumm, and U. Wille, Nucl. Instrum. Methods Phys. Res. B **125**, 273 (1997).

[28] A. H. Makarov, V. T. Platonenko, and V. V. Tyakht, Zh. Eksp. Teor. Fiz. **75**, 2075 (1978).

[29] M. Yu. Gusev, D. V. Klushin, I. F. Urazgil'din, and S. V. Sharov, Zh. Eksp. Teor. Fiz. **103**, 2102 (1993).

[30] H. Shao, D. C. Langreth, and P. Nordlander, Phys. Rev. B **49**, 13 929 (1994).

[31] P. J. Rous, Phys. Rev. Lett. **74**, 1835 (1995).

[32] A. G. Borisov, D. Teillet-Billy, and J. P. Gauyacq, Surf. Sci. **278**, 99 (1992).

[33] See, e.g., in *Time Dependent Methods for Quantum Dynamics*, edited by K. C. Kulander (North-Holland, Amsterdam, 1991).

[34] R. Kosloff, J. Phys. Chem. **92**, 2087 (1988).

[35] J. P. Gauyacq, J. Phys. B **13**, 4417 (1980).

[36] F. Aguillon, M. Sizun, V. Sidis, G. Billing, and N. Markovic, J. Chem. Phys. **104**, 4530 (1990).

[37] D. Lemoine and G. C. Corey, J. Chem. Phys. **94**, 767 (1991).

[38] A. K. Kazansky and K. Taulbjerg, J. Phys. B **29**, 4465 (1996).

[39] A. G. Borisov, A. K. Kazansky, and J. P. Gauyacq, Phys. Rev. Lett. **80**, 1996 (1998).

[40] S. Cohen and G. Fiorentini, Phys. Rev. A **33**, 1590 (1986).

[41] P. J. Jennings, P. O. Jones, and M. Weinert, Phys. Rev. B **37**, 3113 (1988).

[42] M. C. Desjonquères and D. Spanjaard, *Concepts in Surface Physics*, Springer Series in Surface Sciences, Vol. 30 (Springer-Verlag, Berlin, 1993).

[43] P. M. Echenique and J. B. Pendry, Prog. Surf. Sci. **32**, 111 (1990).

[44] E. V. Chulkov, V. M. Silkin, and P. M. Echenique, Surf. Sci. **391**, L1217 (1997).

[45] J. N. M. Van Wunnick, R. Brako, K. Makoshi, and D. M. Newns, Surf. Sci. **126**, 618 (1983).

[46] M. D. Fleit and J. A. Fleck, J. Chem. Phys. **78**, 301 (1982).

[47] C. Leforestier, R. H. Bisseling, C. Cerjan, M. D. Feit, R. Friesner, A. Guldberg, A. Hammerich, G. Jolicard, W. Karrlein, H. D. Meyer, N. Lipkin, O. Roncero, and R. Kosloff, J. Comput. Phys. **94**, 59 (1991).

[48] R. Kosloff, J. Phys. Chem. **92**, 2087 (1988).

[49] J. R. Taylor, *Scattering Theory: The Quantum Theory of Nonrelativistic Collisions* (Krieger, Malabar, FL, 1983).

[50] W. H. Press, S. A. Tenkolsky, W. T. Vetterling, and B. P. Flannery, *Numerical Recipes in FORTRAN* (Cambridge University Press, Cambridge, 1982).

[51] D. Neuhauser and M. Baer, J. Chem. Phys. **91**, 4651 (1989).

[52] T. Seideman and W. H. Miller, J. Chem. Phys. **97**, 2499 (1992).

[53] R. Kosloff and D. Kosloff, J. Comput. Phys. **63**, 363 (1986).

[54] G. Jolicard, C. Leforestier, and E. J. Austin, J. Chem. Phys. **88**, 1026 (1988).

[55] M. R. Wall and J. D. Neuhauser, J. Chem. Phys. **102**, 8011 (1995).

[56] V. A. Mandelshtam and H. S. Taylor, Phys. Rev. Lett. **78**, 3274 (1997).

[57] E. Narevicius, D. Neuhauser, H. J. Korsch, and N. Moiseyev, Chem. Phys. Lett. **276**, 250 (1997).

[58] D. Teillet-Billy and J. P. Gauyacq, Surf. Sci. **269/70**, 162 (1992).

[59] U. Fano, Phys. Rev. **124**, 1866 (1961).

[60] A. K. Kazansky, J. Phys. B **30**, 1401 (1997).

[61] A. K. Kazansky (unpublished).

[62] D. M. Newns, Phys. Rev. **178**, 1123 (1969).

[63] W. Domcke, J. Phys. B **14**, 4889 (1981).

[64] A. Bringer and J. Harris, Surf. Sci. **274**, 403 (1992).

[65] B. Bahrim, A. G. Borisov, D. Teillet-Billy, J. P. Gauyacq, F. Wiegershaus, St. Krischok, and V. Kempter, Surf. Sci. **380**, 556 (1997).

[66] A. G. Borisov, G. E. Makhmetov, B. Bahrim, D. Teillet-Billy, and J. P. Gauyacq, Nucl. Instrum. Methods Phys. Res. B **125**, 242 (1997).

[67] J. P. Gauyacq and A. G. Borisov, J. Phys.: Condens. Matter **10**, 6585 (1998).

[68] A. Borisov and H. Winter, Z. Phys. D **37**, 263 (1996).

[69] Q. Yan, J. Burgdörfer, and F. W. Meyer, Phys. Rev. B **56**, 1589 (1997).